

PREPARATION OF YB-DOPED SRCEO₃ SPUTTER TARGETS FOR PROTONIC SOLID OXIDE FUEL CELLS

Fatih Pişkin*, Department of Metallurgical and Materials Engineering, Faculty of Engineering, Muğla Sıtkı Koçman University, Turkey, fatihpisikin@mu.edu.tr

() <https://orcid.org/0000-0002-5321-0381>

Received: 04.11.2021, Accepted: 18.01.2022

Research Article

*Corresponding Author

DOI: 10.22531/muglajsci.1019127

Abstract

A comprehensive study was carried out starting from powder synthesis to sintering procedure in order to produce a phase-pure SrCe_{0.95}Yb_{0.05}O_{3-δ} sputter target. In the powder synthesis, the effect of chelating and polymerization agents on the formation of single-phase SrCe_{0.95}Yb_{0.05}O_{3-δ} was investigated in detail. In this regard, citric acid, EDTA, and their combinations in different ratios were evaluated as chelating agents. The calcination temperature, ranging from 1000 °C to 1300 °C, was also investigated to reveal its effect on the formation of possible secondary phases. Following the powder synthesis, SrCe_{0.95}Yb_{0.05}O_{3-δ} sputter target with dimensions of ~50 mm diameter and ~3 mm thickness was produced by powder pressing with deformable compaction die and the subsequent sintering at 1300 °C for 10 hours. A relative density of 0.95 was achieved in SrCe_{0.95}Yb_{0.05}O_{3-δ} targets as a result of the procedure in question without the use of a sintering aid.

Keywords: Yb-doped SrCeO₃, Deformable compaction die, Sintering, Sputter deposition, Thin film.

PROTONİK KATI OKSİT YAKIT HÜCRELERİ İÇİN YB KATKILI SRCEO₃ SİÇRATMA HEDEF MALZEMELERİNİN HAZIRLANMASI

Özet

Tek fazlı SrCe_{0.95}Yb_{0.05}O_{3-δ} sıçratma hedefi üretmek amacıyla toz sentezi ve sinterleme işlemlerini içeren kapsamlı bir çalışma gerçekleştirilmiştir. Toz sentezinde, şelatlayıcı ve polimerizasyon ajanlarının tek fazlı SrCe_{0.95}Yb_{0.05}O_{3-δ} oluşumuna etkisi detaylı olarak incelenmiştir. Bu bağlamda şelatlayıcı ajan olarak sitrik asit, EDTA ve bunların farklı oranlardaki kombinasyonları değerlendirilmiştir. SrCe_{0.95}Yb_{0.05}O_{3-δ} sentezinde, kalsinasyon sıcaklığının ikincil faz oluşumu üzerindeki etkisini de ortaya koymak amacıyla 1000 °C ile 1300 °C arasında değişen kalsinasyon sıcaklıkları çalışmada ayrıca ele alınmıştır. Yaklaşık 50 mm çap ve 3 mm kalınlığa sahip SrCe_{0.95}Yb_{0.05}O_{3-δ} sıçratma hedefi, deforme olabilir sıkıştırma kalıbı kullanılarak toz presleme ve takiben 1300 °C'de 10 saat süre ile gerçekleştirilen sinterleme işlemi ile üretilmiştir. Çalışmada ele alınan yöntem ile herhangi bir sinterleme yardımcısı kullanılmadan 0.95 nispi yoğunluğa sahip tek fazlı SrCe_{0.95}Yb_{0.05}O_{3-δ} sıçratma hedefi elde edilmiştir.

Anahtar Kelimeler: Yb katkılı SrCeO₃, Deforme edilebilir sıkıştırma kalıbı, Sinterleme, Saçtırmalı biriktirme, İnce film.

Cite

Pişkin, F., (2022). "Preparation Of Yb-doped SrCeO₃ Sputter Targets for Protonic Solid Oxide Fuel Cells", *Mugla Journal of Science and Technology*, 8(1), 1-7.

1. Introduction

Perovskite-type oxides with mixed electronic and protonic conductivity (MEPC) have been extensively studied for their potential use as an essential component in several applications such as electrolyzers [1,2], separation membranes [3,4], and solid oxide fuel cells (SOFCs) [5–8]. Among these oxides, SrCeO₃ and BaCeO₃, having ABO₃ structure, are quite attractive due to their high proton conductivity at temperatures ranging from 600-1000 °C. However, it has been reported that BaCeO₃-based oxides also exhibit a remarkable oxygen conductivity depending on oxygen partial pressure and water vapor in the ambient atmosphere [9]. This, therefore, limits the use of BaCeO₃-based oxides as

electrolytes for protonic SOFCs or as membranes for hydrogen separation [10]. On the other hand, SrCeO₃-based oxides could offer sole proton conductivity under operating conditions of SOFCs and the membranes used for the purification of hydrogen from the gas mixtures.

MEPC in these types of oxides is typically achieved by doping with aliovalent dopants resulting in the formation of defects in complex oxide structures [11]. There are various ways of synthesis methods such as solid-state reaction [12], sol-gel [13], and Pechini synthesis [14] in order to maintain these complex structures. However, regardless of the method adopted, the production of single-phase perovskite structures without the formation

of a secondary phase could be problematic and require extensive and coordinated works. The possible impurities such as oxides derivatives of the compounds can be formed during the synthesis and could result in a performance degradation [15] or a chemical instability [13] in these oxides. Thus, controlling the synthesis conditions is quite critical for the elimination of any possible impurity.

As an extensive property, the thickness of the electrolytes or the membranes is another factor that affects the overall performance of these oxides in practical applications. It has been reported that the use of thin-film electrolytes in protonic SOFCs would reduce the ohmic polarization and increase the rate of reaction kinetics [16]. This often allows the electrolytes to operate at lower temperatures. It was also reported that 10^2 - 10^3 times higher conductivity could be achieved in thin-film proton-conducting electrolytes with respect to their bulk equivalents [17,18]. The increase in total conductivity with reduced thickness was typically attributed to surface conduction together with the grain and grain boundary structures formed in the thin films. It has been, similarly, reported that the thickness reduction in separation membranes also resulted in enhanced hydrogen fluxes as the flux is inversely proportional to membrane thickness [19]. Therefore, the thin film proton conductors are quite attractive and have been studied extensively due to their enhanced performances.

It is known that each deposition technique requires the use of a source or a target material in order to enable film growth. It would normally be expected that the source/target material transposes its characteristic features such as composition, structure, and phase purity to the film deposited during the deposition. For example, sputter targets, having a high relative density (>0.90), are required for thin-film sputter deposition, otherwise, insufficient density and residual pores in the targets cause interruptions in the glow discharge during deposition, and the formation of inhomogeneous compositions on the thin films deposited [20]. Therefore, the production of the target materials is critical since targets/sources directly affect the quality of thin film deposited.

Achieving high relative densities in targets, particularly in oxides such as SrCeO₃ having high sintering temperatures (>1300 °C) could be challenging. These oxides typically require the use of sintering aids in order to reduce the sintering temperatures and increase the relative density that could be achieved. However, the use of sintering aids such as SrO or ZnO results in residual secondary phases in the host structure. This might reduce the total conductivity of these types of oxides [21,22]. Therefore, there is a need for sintering approaches that offer high relative density at low sintering temperatures without the use of sintering aids.

The current study focus on the production of phase-pure sputter target for thin film deposition of Yb-doped SrCeO₃, i.e. SrCe_{0.95}Yb_{0.05}O₃, one of the perovskite-type oxide offering high proton conductivity and used as a solid electrolyte for protonic SOFCs [23,24]. In this regard, the effect of chelating and polymerization agents on the Pechini synthesis of SrCe_{0.95}Yb_{0.05}O₃ (SCY) was investigated. The effect of citric acid (CA) and ethylenediaminetetraacetic acid (EDTA) as chelating agents were compared with different fractions, while ethylene glycol (EG) was preferred as a polymerization agent. The effect of calcination temperature, ranging between 1000°C and 1300°C, on the formation of secondary phases was also investigated. In the current study, the SCY sputtering target with a theoretical density of 95% was produced using a deformable compaction die and subsequent sintering procedure without the use of sintering aids.

2. Experimental Studies

2.1. Powder Synthesis

SrCe_{0.95}Yb_{0.05}O_{3-δ} (SCY) were synthesized by the Pechini method [25] using nitrate salts of the metal cations, i.e. Sr(NO₃)₂ (Alfa Aesar 99.0%), Ce(NO₃)₃·6H₂O (Merck≥98.5%), and Yb(NO₃)₃·14H₂O (Alfa Aesar 99.9%). CA (Carlo Erba 99.5%), and EDTA (Carlo Erba ≥99.0%) were preferred as chelating agents, while EG (Carlo Erba ≥99.5%) was used as a polymerization agent. The applied molar ratio between total metal cation (TM), CA, EDTA, and EG is given in Table 1. During the course of syntheses, nitrate salts were first dissolved in an adequate amount of de-ionized water at 300 rpm by magnetic stirring. The solutions were then continuously stirred at 70 °C until the viscous gel formed. The gel was dried at 250 °C in an oven for 2h. Black powders, obtained with this procedure, were calcined for 5 h at temperatures ranging between 1000 °C and 1200 °C in stagnant air to remove residual organics and to form the perovskite structure.

2.2. Powder Pressing by Deformable Compaction Die

Compaction of SCY powders was carried out using a uniaxial hydraulic press. Deformable compaction dies made of PTFE with dimensions of 5 mm height, 5 mm thickness, and a diameter ranging between 60 mm and 68 mm were employed to achieve ideal dimensions for sputter target after sintering, i.e. 50 mm diameter and 3 mm thickness. SCY powders were compacted with pressures from 50 MPa to 150 MPa with 25 MPa increments. Following the compaction of green pellets, the sintering procedure was carried out in a box furnace at 1300 °C for 10 h with a constant heating/cooling rate of 2 °C/min. The density of green and sintered pellets were measured with the Archimedes method [26].

2.3. Thin Film Sputter Deposition of SrCe_{0.95}Yb_{0.05}O₃

Thin-film sputter deposition of SCY, using the target produced with the applied procedure, was carried out in

a custom-configured magnetron sputtering system [27–31]. The system has RF sputter guns accommodating targets in 50 mm diameter. Therefore, a 50 mm diameter was accordingly aimed for the pellets in the current study. SCY thin films were deposited on glass substrates having dimensions of 18 mm diameter and approximately 100 μm thickness. The substrates were heated to 400 °C before the deposition. 100 watts of RF power was applied to the SCY target that yielded a deposition rate of 0.35-0.40 Å/s at 2.50 mTorr argon pressure. The deposition was carried out for almost 12 h to test the sputter target produced in the work.

2.4. Chemical and Structural Characterization

Phase analysis of the synthesized powders, SCY target, and SCY thin films was carried out by a Rigaku SmartLab X-ray diffractometer. X-ray diffraction (XRD) analyses were performed using Cu-Kα radiation (λ= 1,5406 Å) in Bragg-Brentano geometry. XRD patterns were processed by the Rietveld refinement method [32] using MAUD software [33] to obtain crystallographic information.

The chemical composition of synthesized powders was determined by ICP-OES analysis using a Perkin Elmer Optima 4300DV. A JEOL JSM-7600F scanning electron microscope (SEM) was used in secondary electron imaging mode at accelerating voltage ranging between 10 and 20 kV for the investigation of microstructure and morphology of the oxides.

3. Results and Discussion

Figure 1 and Figure 2 display the XRD patterns of SCY powders synthesized with different TM:CA:EDTA:EG ratios and calcined at 1100 °C and 1200 °C for 5 h. XRD patterns of SCY powders calcined at 1000 °C are not included in the figures as they had a relatively high amount of secondary phases, i.e. oxide derivatives of Ce and non-stoichiometric SCY.

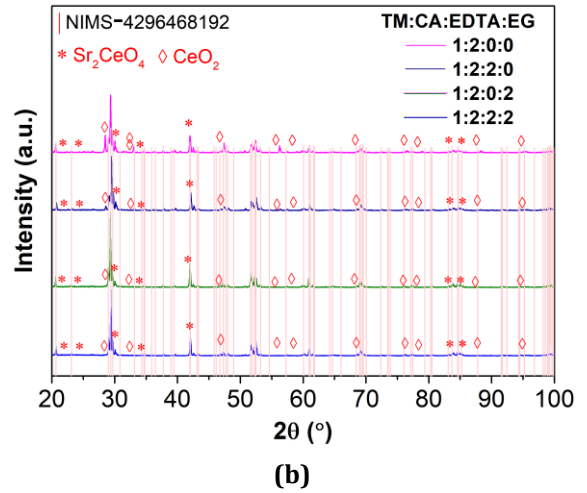


Figure 1. XRD patterns of SCY powders synthesized with the TM:CA:EDTA:EG ratio of 1:2:0:0, 1:2:2:0, 1:2:0:2, 1:2:2:2 calcined at (a) 1100 °C and (b) 1200 °C for 5 h. The stick pattern of cubic SCY, NIMS-4296468192, is also added to the figures.

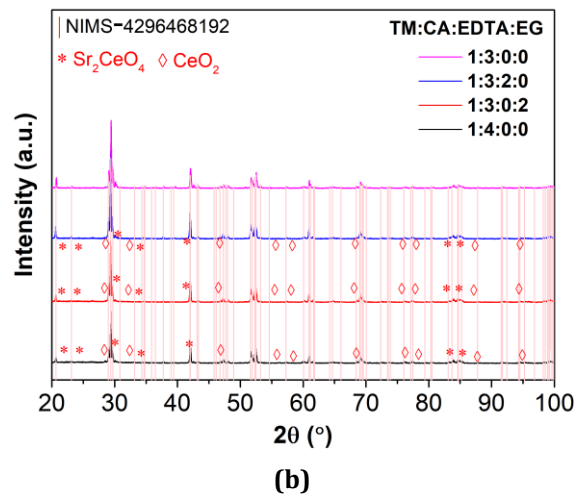
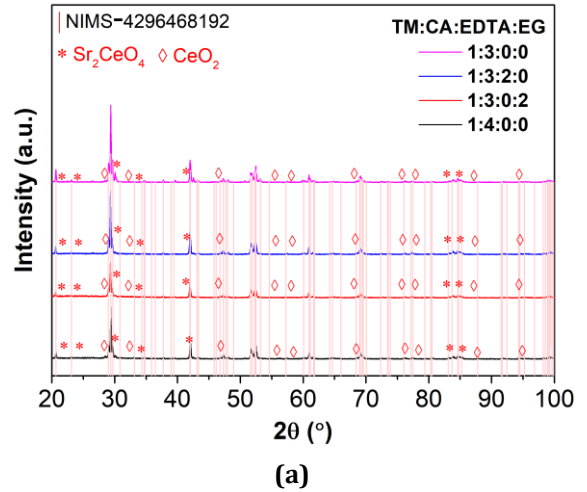


Figure 2. XRD patterns of SCY powders synthesized with the TM:CA:EDTA:EG ratio of 1:3:0:0, 1:3:2:0, 1:3:0:2, 1:4:0:0 calcined at (a) 1100 °C and (b) 1200 °C for 5 h. The stick pattern of cubic SCY, NIMS-4296468192, is also added to the figures.

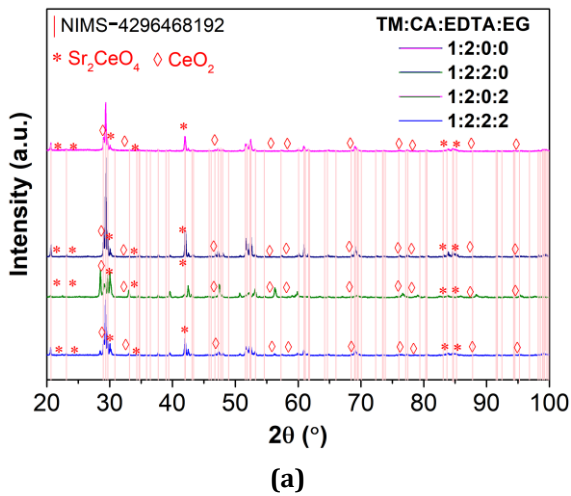


Table 1. TM:CA:EDTA:EG ratios applied during SCY synthesis. The secondary phases formed after calcination at temperatures between 1000 °C to 1200 °C for 5 h are included in the table. Weighted residual values (Rwp) in the Rietveld refinements were obtained less than 15% for each analysis.

TM:CA:EDTA:EG	Calcination Temperature		
	1000 °C	1100 °C	1200 °C
1:2:0:0	Sr ₂ CeO ₄ =2.52% CeO ₂ =4.48	Sr ₂ CeO ₄ =10.63% CeO ₂ =1.87%	Sr ₂ CeO ₄ =2.35% CeO ₂ =0.90%
1:2:2:0	Sr ₂ CeO ₄ =23.84% CeO ₂ =14.21%	Sr ₂ CeO ₄ =20.31% CeO ₂ =4.97%	Sr ₂ CeO ₄ =16.31% CeO ₂ =0.54%
1:2:0:2	Sr ₂ CeO ₄ =27.39% CeO ₂ =22.94%	Sr ₂ CeO ₄ =25.12% CeO ₂ =12.55%	Sr ₂ CeO ₄ =28.54% CeO ₂ =3.40%
1:2:2:2	Sr ₂ CeO ₄ =25.39% CeO ₂ =24.94%	Sr ₂ CeO ₄ =17.12% CeO ₂ =3.55%	Sr ₂ CeO ₄ =15.54% CeO ₂ =3.13%
1:3:0:0	Sr ₂ CeO ₄ =1.45% CeO ₂ =-	SCY	Sr ₂ CeO ₄ =- CeO ₂ =2.52%
1:3:2:0	Sr ₂ CeO ₄ =21.65% CeO ₂ =6.71%	Sr ₂ CeO ₄ =15.85% CeO ₂ =5.11%	Sr ₂ CeO ₄ =14.34% CeO ₂ =2.98%
1:3:0:2	Sr ₂ CeO ₄ =22.47% CeO ₂ =4.84%	Sr ₂ CeO ₄ =17.71% CeO ₂ =1.84%	Sr ₂ CeO ₄ =6.51% CeO ₂ =1.64%
1:4:0:0	Sr ₂ CeO ₄ =3.22% CeO ₂ =0.70%	Sr ₂ CeO ₄ =1.17% CeO ₂ =1.20%	Sr ₂ CeO ₄ =2.51% CeO ₂ =1.92%

XRD patterns display that the calcination at 1100 °C dominantly resulted in the formation of crystalline cubic SCY. However, there was a remarkable amount of secondary phases, i.e. Sr₂CeO₄ and CeO₂. The formation of secondary phases is almost independent of the synthesis parameters employed for 1100 °C. It was observed that the use of EG typically drives the formation of particularly Sr₂CeO₄ to a higher extend. All synthesis conditions, except TM:CA 1:3, yielded these undesired phases. The amount of the phases in the powders synthesized was calculated by Rietveld refinement with MAUD software [34] and given in Table 1. Among the synthesis conditions studied in the work, only TM:CA 1:3 resulted in phase-pure SCY without any detectable secondary phase. The further increment in CA ratio, i.e. TM:CA 1:4 yielded the formation of Sr₂CeO₄ and CeO₂.

The higher calcination temperature, i.e. 1200 °C resulted in secondary phase formation even with TM:CA 1:3. This ratio yielded a limited amount of CeO₂ in the case of calcination at 1200 °C. Thus, the synthesis condition to produce phase-pure SCY was determined as TM:CA 1:3 and the calcination temperature as 1100 °C.

The morphology of the phase-pure SCY powders synthesized with TM:CA 1:3 ratio was investigated by SEM in secondary electron imaging mode after calcination, and the micrographs are given in Figure 3.

Micrographs display that the synthesis with TM:CA 1:3 ratio typically yielded equiaxed particles having sizes of less than 500 nm. Micrographs also indicated that the powders synthesized with the selected conditions were tended to sinter at 1100 °C.

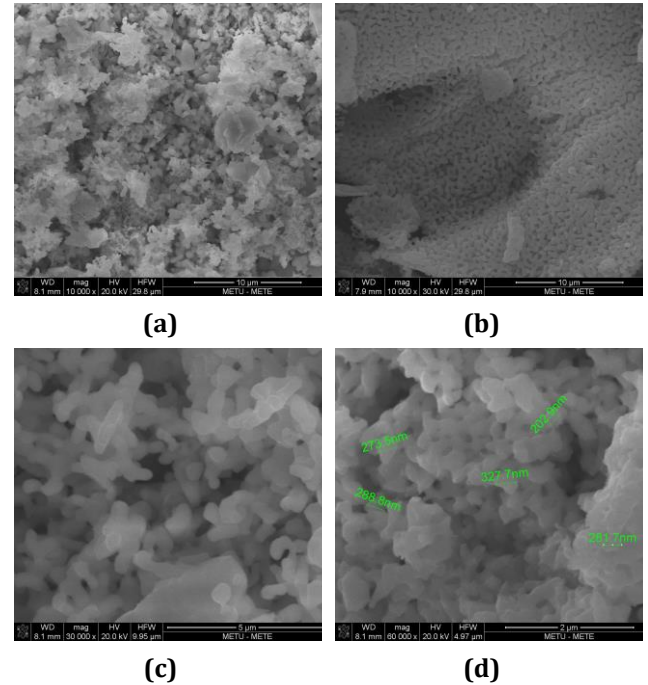


Figure 3. SEM micrographs of SCY powders at (a), (b) 1000X magnification, (c) 30000X magnification and (d) 60000X magnification. SCY powders were synthesized with TM:CA 1:3 ratio and calcined at 1100 °C for 5h.

Subsequently, powder pressing was carried out using the synthesized SCY powders under a pressure ranging from 50 MPa to 150 MPa with increments of 25 MPa. The density of green pellets was measured by the Archimedes method and is given in Figure 4. As expected, the density of green pellets increased with an increase in the applied pressure. The highest green density, i.e. 0.72 was achieved with 150 MPa applied pressure.

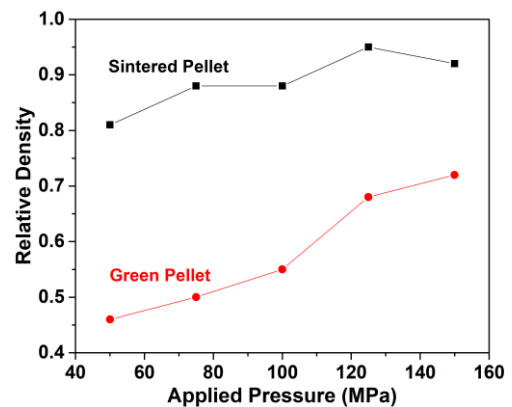


Figure 4. Relative density change in green and sintered SCY (theoretical density, 5.66 g/cm³) pellets.

Each pellet was then sintered at the same conditions, i.e. under stagnant air at 1300 °C for 10 h. The density of sintered pellets was similarly measured. The sintered density of the pellets is also included in Figure 4. The relative density of sintered pellets increased with increasing pressure and reached up to 0.95 with 125 MPa applied pressure. This high relative density of 0.95 was achieved with a single-step procedure adopted in the study. This result is comparable with other studies, which are typically using some sintering aids and have multi-step heat treatments in order to achieve such a high relative density [35,36].

The further increment in applied pressure, i.e. 150 MPa resulted in a reduction in the final density. The pellet pressed at 150 MPa yielded a sintered density of 5.20 g/cm³ that is approximately 0.92 of its true density. The reduction in density with higher applied pressure is actually in good agreement with the previous works [37]. This lower density obtained with higher compaction pressure is often explained by the voids trapped in the relatively dense green compact that could not be released during sintering.

SCY pellet, pressed at 125 MPa and sintered at 1300 °C for 10 h, was then investigated by SEM. A representative micrograph of the pellet is given in Figure 5.

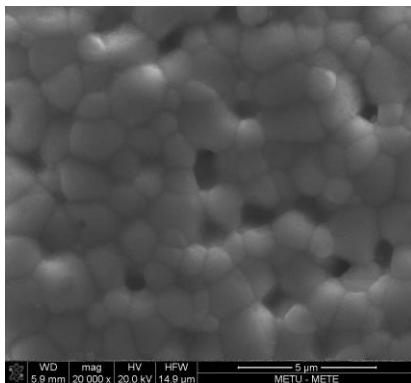


Figure 5. SEM micrograph of SCY pellet pressed at 125 MPa and sintered at 1300 °C for 10 h.

Here, the micrograph of the pellet displays remarkable densification although some remaining surface pores yielded a relative density of 0.95.

SCY pellet was also investigated by XRD in order to confirm the presence of the phases in the pellet following the sintering procedure. The XRD pattern given in Figure 6 shows that there is not any secondary phase that could be detected in XRD. This indicated the phase-pure SCY could be maintained upon 10 h of sintering at 1300 °C. It can be concluded that the applied methodology yielded a SCY target material satisfying the requirements in terms of chemical, structural, and density.

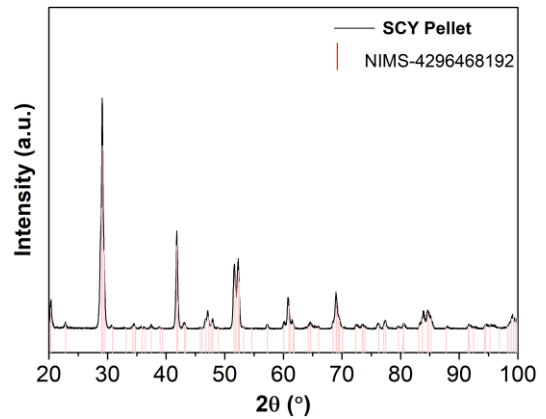
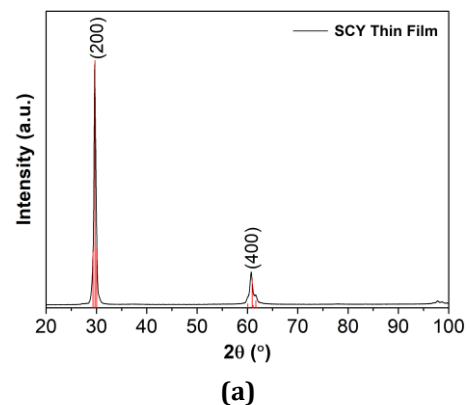
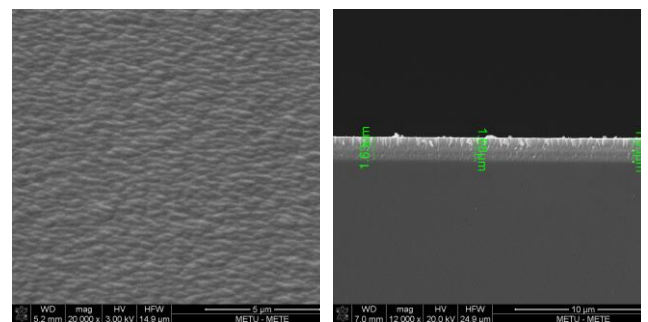


Figure 6. XRD pattern of SCY pellet pressed at 125 MPa and sintered at 1300 °C for 10 h.

SCY sputter target produced was tested in a magnetron sputtering system for thin film deposition. Sputter deposition of SCY was carried out at 100W RF for 12 h. Subsequent to deposition, any sign of crack or failure was not detected in the target. This indicated that the target prepared can withstand the thermal shocks during the sputter deposition.



(a)



(b)

(c)

Figure 7. (a) XRD pattern of SCY thin film exhibiting strong (200) pseudo-cubic preferred orientation upon sputter deposition. (b) Morphology of SCY thin film produced by sputter deposition. Micrograph showed that pore-free and continuous SCY film could be deposited using the target material produced in the present work. (c) The cross-section view of SCY film showed that ~1.60 μm thickness was achieved with 100 watts of RF power applied for 12 h.

SCY thin films were also investigated by SEM and XRD to identify their morphology and structure. XRD analysis indicated that highly textured crystalline SCY films were deposited on glass substrates. The patterns revealed that SCY films exhibited a strong preferred orientation in the (200) plane, Figure 7 (a). SEM micrographs displayed that SCY thin films were uniform and free from voids, Figure 7 (b). The cross-section micrographs of the thin films also confirmed that fully dense SCY films could be deposited with the target produced in the study, Figure 7 (c).

4. Conclusions

In order to fabricate a phase-pure SCY sputter target with a high relative density, systematic work was carried out. Initially, ideal synthesis parameters were determined so as to obtain phase-pure SCY powders. TM:CA ratio of 1:3 enabled the synthesis of phase-pure and crystalline SCY powders having sub-micron sizes. SCY pellets were then produced using deformable compaction die made of PTFE. During the course compaction, pressures from 50 MPa to 150 MPa with increments of 25 MPa were applied and the pellets were then sintered at the same conditions, i.e. at 1300 °C for 10 h. The maximum relative density of 0.95 was achieved in sintered SCY pellet with 125 MPa, while further increment in applied pressure resulted in a decrease in relative density. SCY target was tested for a thin film deposition in a magnetron sputtering system for 12 h. There was no cracking or failure in the target during the course of sputter deposition. These results together with SEM and XRD analyses indicated that the SCY sputter target produced with the applied methodology meets the requirements of a sputter target in terms of chemical composition, structure, and density.

5. Acknowledgment

This work was funded by TUBITAK under project number 119M065, which the authors gratefully acknowledge.

6. References

- [1] Vøllestad, E., Strandbakke, R., Tarach, M., Catalán-Martínez, D., Fontaine, M.-L., Beeaff, D., Clark, D. R., Serra, J. M., and Norby, T., "Mixed proton and electron conducting double perovskite anodes for stable and efficient tubular proton ceramic electrolyzers," *Nature Materials*, vol. 18, no. 7, pp. 752–759, 2019.
- [2] Choi, S., Davenport, T. C., and Haile, S. M., "Protonic ceramic electrochemical cells for hydrogen production and electricity generation: exceptional reversibility, stability, and demonstrated faradaic efficiency," *Energy & Environmental Science*, vol. 12, no. 1, pp. 206–215, 2019.
- [3] Hashim, S. S., Somalu, M. R., Loh, K. S., Liu, S., Zhou, W., and Sunarso, J., "Perovskite-based proton conducting membranes for hydrogen separation: A review," *International Journal of Hydrogen Energy*, vol. 43, no. 32, pp. 15281–15305, 2018.
- [4] Wang, H., Wang, X., Meng, B., Tan, X., Loh, K. S., Sunarso, J., and Liu, S., "Perovskite-based mixed protonic–electronic conducting membranes for hydrogen separation: Recent status and advances," *Journal of Industrial and Engineering Chemistry*, vol. 60, pp. 297–306, 2018.
- [5] Wei, Z., Wang, J., Yu, X., Li, Z., Zhao, Y., and Chai, J., "Study on Ce and Y co-doped BaFeO_{3-δ} cubic perovskite as free-cobalt cathode for proton-conducting solid oxide fuel cells," *International Journal of Hydrogen Energy*, vol. 46, no. 46, pp. 23868–23878, 2021.
- [6] Cao, Y., Dhahad, H. A., Sun, Y.-L., Abdollahi Haghghi, M., Delpisheh, M., Athari, H., and Farouk, N., "The role of input gas species to the cathode in the oxygen-ion conducting and proton conducting solid oxide fuel cells and their applications: Comparative 4E analysis," *International Journal of Hydrogen Energy*, vol. 46, no. 37, pp. 19569–19589, 2021.
- [7] An, H., Lee, H.-W., Kim, B.-K., Son, J.-W., Yoon, K. J., Kim, H., Shin, D., Ji, H.-I., and Lee, J.-H., "A 5 × 5 cm² protonic ceramic fuel cell with a power density of 1.3 W cm⁻² at 600 °C," *Nature Energy*, vol. 3, no. 10, pp. 870–875, 2018.
- [8] Okuyama, Y., Okuyama, K., Mizutani, Y., Sakai, T., Lee, Y. S., and Matsumoto, H., "Proton transport properties of La_{0.9}Sr_{0.1}Yb_{0.8}In_{0.2}O_{3-δ} and its application to proton ceramic fuel cell," *International Journal of Hydrogen Energy*, vol. 39, no. 35, pp. 20829–20836, 2014.
- [9] Souza, E. C. C. de and Muccillo, R., "Properties and applications of perovskite proton conductors," *Materials Research*, vol. 13, no. 3, pp. 385–394, 2010.
- [10] Mather, G. C., Poulidi, D., Thursfield, A., Pascual, M. J., Jurado, J. R., and Metcalfe, I. S., "Hydrogen-permeation characteristics of a SrCeO₃-based ceramic separation membrane: Thermal, ageing and surface-modification effects," *Solid State Ionics*, vol. 181, no. 3–4, pp. 230–235, 2010.
- [11] Xing, W., Inge Dahl, P., Valland Roaas, L., Fontaine, M.-L., Larring, Y., Henriksen, P. P., and Bredesen, R., "Hydrogen permeability of SrCe_{0.7}Zr_{0.25}Ln_{0.05}O_{3-δ} membranes (Ln=Tm and Yb)," *Journal of Membrane Science*, vol. 473, pp. 327–332, 2015.
- [12] Taglieri, G., Tersigni, M., Villa, P., and Mondelli, C., "Synthesis by the citrate route and characterisation of BaZrO₃, a high tech ceramic oxide: preliminary results," *International Journal of Inorganic Materials*, vol. 1, no. 1, pp. 103–110, 1999.
- [13] D'Epifanio, A., Fabbri, E., Di Bartolomeo, E., Licocchia, S., and Traversa, E., "BaZr_xY_{1-x}O_{3-d} and BaCe_{1-x}Zr_xY_zO_{3-d} Proton Conductors For

- Intermediate Temperature Solid Oxide Fuel Cells (IT-SOFCs)," *ECS Transactions*, vol. 7, no. 1, pp. 2337–2342, 2019.
- [14] Meng, B., "Synthesis and characterization of SrCe_{0.95}Y_{0.05}O₃ nano powders by low temperature combustion," *Rare Metals*, vol. 25, no. 1, pp. 79–83, 2006.
- [15] Iguchi, F., Tsurui, T., Sata, N., Nagao, Y., and Yugami, H., "The relationship between chemical composition distributions and specific grain boundary conductivity in Y-doped BaZrO₃ proton conductors," *Solid State Ionics*, vol. 180, no. 6–8, pp. 563–568, 2009.
- [16] Fallah Vostakola, M. and Amini Horri, B., "Progress in Material Development for Low-Temperature Solid Oxide Fuel Cells: A Review," *Energies*, vol. 14, no. 5, p. 1280, 2021.
- [17] Pornprasertsuk, R., Kosasang, O., Somroop, K., Horprathum, M., Limnonthakul, P., Chindaudom, P., and Jinawath, S., "Proton conductivity of Y-doped BaZrO₃: Pellets and thin films," *Solid State Sciences*, vol. 13, no. 7, pp. 1429–1437, 2011.
- [18] Droushiotis, N., Grande, F. D., Dzarfan Othman, M. H., Kanawka, K., Doraswami, U., Metcalfe, I. S., Li, K., and Kelsall, G., "Comparison Between Anode-Supported and Electrolyte-Supported Ni-CGO-LSCF Micro-tubular Solid Oxide Fuel Cells," *Fuel Cells*, vol. 14, no. 2, pp. 200–211, 2014.
- [19] Yoon, H., Song, S.-J., Oh, T., Li, J., Duncan, K. L., and Wachsmann, E. D., "Fabrication of Thin-Film SrCe_{0.9}Eu_{0.1}O_{3-δ} Hydrogen Separation Membranes on Ni-SrCeO₃ Porous Tubular Supports," *Journal of the American Ceramic Society*, vol. 92, no. 8, pp. 1849–1852, 2009.
- [20] Lo, C.-C. and Hsieh, T.-E., "Preparation of IGZO sputtering target and its applications to thin-film transistor devices," *Ceramics International*, vol. 38, no. 5, pp. 3977–3983, 2012.
- [21] Duval, S. B. C., Holtappels, P., Stimming, U., and Graule, T., "Effect of minor element addition on the electrical properties of BaZr_{0.9}Y_{0.1}O_{3-δ}," *Solid State Ionics*, vol. 179, no. 21–26, pp. 1112–1115, 2008.
- [22] Babilo, P. and Haile, S. M., "Enhanced Sintering of Yttrium-Doped Barium Zirconate by Addition of ZnO," *Journal of the American Ceramic Society*, vol. 88, no. 9, pp. 2362–2368, 2005.
- [23] Zhang, W. and Hu, Y. H., "Progress in proton-conducting oxides as electrolytes for low-temperature solid oxide fuel cells: From materials to devices," *Energy Science & Engineering*, vol. 9, no. 7, pp. 984–1011, 2021.
- [24] Baker, R. T., Salar, R., Potter, A. R., Metcalfe, I. S., and Sahibzada, M., "Influence of morphology on the behaviour of electrodes in a proton-conducting Solid Oxide Fuel Cell," *Journal of Power Sources*, vol. 191, no. 2, pp. 448–455, 2009.
- [25] Pechini, M. P., "Method of preparing lead and alkaline earth titanates and niobates and coating method using the same to form a capacitor," 3,330,697, 1967
- [26] ASTM International, "Standard Test Methods for Density of Compacted or Sintered Powder Metallurgy (PM) Products Using Archimedes' Principle," *Astm B962-13*, 2013..
- [27] Pişkin, F. and Öztürk, T., "Nb-Pd-Ti BCC thin films for hydrogen separation," *Journal of Alloys and Compounds*, vol. 775, pp. 411–418, 2019.
- [28] Pişkin, F., Akyıldız, H., and Öztürk, T., "Ti modified Pd–Ag membranes for hydrogen separation," *International Journal of Hydrogen Energy*, vol. 40, no. 24, pp. 7553–7558, 2015.
- [29] Pişkin, F. and Öztürk, T., "Combinatorial screening of Pd-Ag-Ni membranes for hydrogen separation," *Journal of Membrane Science*, vol. 524, pp. 631–636, 2017.
- [30] Sarı, D., Yaşar, B., Pişkin, F., Kalay, Y. E., and Öztürk, T., "Segregation Resistant Nanocrystalline/Amorphous (La,Sr)CoO₃-(La,Sr)₂CoO₄ Composite Cathodes for IT-SOFCs," *Journal of The Electrochemical Society*, vol. 166, no. 15, pp. F1157–F1163, 2019.
- [31] Sarı, D., Pişkin, F., Torunoğlu, Z. C., Yaşar, B., Kalay, Y. E., and Öztürk, T., "Combinatorial development of nanocrystalline/amorphous (La,Sr)CoO₃-(La,Sr)₂CoO₄ composite cathodes for IT-SOFCs," *Solid State Ionics*, vol. 326, pp. 124–130, 2018.
- [32] Rietveld, H. M., "A profile refinement method for nuclear and magnetic structures," *Journal of Applied Crystallography*, vol. 2, no. 2, pp. 65–71, 1969.
- [33] Lutterotti, L., Chateigner, D., Ferrari, S., and Ricote, J., "Texture, residual stress and structural analysis of thin films using a combined X-ray analysis," *Thin Solid Films*, vol. 450, no. 1, pp. 34–41, 2004.
- [34] Ischia, G., Wenk, H.-R., Lutterotti, L., and Berberich, F., "Quantitative Rietveld texture analysis of zirconium from single synchrotron diffraction images," *Journal of Applied Crystallography*, vol. 38, no. 2, pp. 377–380, 2005.
- [35] Dahl, P. I., Haugsrud, R., Lein, H. L., Grande, T., Norby, T., and Einarsrud, M.-A., "Synthesis, densification and electrical properties of strontium cerate ceramics," *Journal of the European Ceramic Society*, vol. 27, no. 16, pp. 4461–4471, 2007.
- [36] Minhui, Z., Xiuxin, Z., and Zhigang, Z., "Preparation and Characterization of Yb Doped SrCeO₃ Based High Temperature Proton Conductor," *Chinese Journal of Engineering*, vol. 15, no. 3, pp. 310–315, 1993.
- [37] Ning, Z., Da-Ming, Z., and Gong, Z., "An investigation on preparation of CIGS targets by sintering process," *Materials Science and Engineering: B*, vol. 166, no. 1, pp. 34–40, 2010.